NRC Publications Archive
Archives des publications du CNRC

Profiling brain function : Spatiotemporal characterization of normal and abnormal visual activation

Versteeg, Vanessa L.; Marchand, Yannick; Mazerolle, Erin L.; D'Arcy, Ryan C. N.

NRC Publications Record / Notice d'Archives des publications de CNRC:
https://nrc-publications.canada.ca/eng/view/object/?id=9190f837-98fd-4b46-8039-bfd873f5dbcf
https://publications-cnrc.canada.ca/fra/voir/objet/?id=9190f837-98fd-4b46-8039-bfd873f5dbcf

Questions? Contact the NRC Publications Archive team at
PublicationsArchive-ArchivesPublications@nrc-cnrc.gc.ca. If you wish to email the authors directly, please see the first page of the publication for their contact information.

Vous avez des questions? Nous pouvons vous aider. Pour communiquer directement avec un auteur, consultez la première page de la revue dans laquelle son article a été publié afin de trouver ses coordonnées. Si vous n'arrivez pas à les repérer, communiquez avec nous à PublicationsArchive-ArchivesPublications@nrc-cnrc.gc.ca.

National Research Council Canada   Conseil national de recherches Canada

Canada

Profiling brain function: Spatiotemporal characterization of normal and abnormal visual activation

Versteeg, Vanessa L.; Marchand, Yannick; Mazerolle, Erin L.; D'Arcy, Ryan C. N.

Abstract

Objective

In clinical neuroscience, the utility of evoked and event-related potentials (EPs and ERPs) resides in the temporal information they provide. However, it is largely unknown whether valuable diagnostic information resides within the corresponding spatial patterns. To determine this, the first step involves testing whether "normal" versus "abnormal" EPs/ERPs can be differentiated based on spatial patterns. In the current study, we present a method that characterizes similarities across individual source maps, called the profile algorithm. The profile algorithm was evaluated in terms of its ability to detect spatial activation differences in myopic individuals with corrected and uncorrected vision. This experiment represents a critical test of the method before applying it to the assessment of perceptual/cognitive functions.

Methods

Visual-evoked potentials (VEPs) were recorded from healthy subjects using checkerboard stimulation. The N75 and P100 were examined in individuals with corrected (20/20) and uncorrected vision (20/40 or worse).

Results and conclusion

N75 and P100 amplitudes and latencies were modulated by vision condition. The profile algorithm differentiated successfully between corrected and uncorrected vision. Its discriminatory power outperformed a more traditional method based on ERP peak amplitude. Subsequent correlations revealed significant relationships between visual impairment and both the components and the spatial activation. Overall, the findings suggested that VEP spatial patterns were sensitive to manipulations of visual acuity.

Significance

The findings demonstrate that EP/ERP spatial activation can be evaluated at the individual level and compared against normative data. Ultimately, the method may provide a valuable tool for assessing individual spatial activation changes in perceptual/cognitive functions.

Keywords: Visual-evoked potentials (VEPs); Event-related brain potentials (ERPs); Source localization; Individual analysis; Vision impairment; Clinical assessment

1. Introduction

1.1. Overview

Electroencephalography (EEG) has a wide variety of research and clinical applications in neuroscience. For instance, evoked and event-related potentials (EPs and ERPs) are signal-averaged derivatives of EEG with well-established strengths in temporal resolution for neural processing (Luck, 2005). Consequently, the temporal resolution of EPs and ERPs has led to a number of clinical applications in neurology and neuropsychology ([Chiappa, 1997] and [Connolly and D'Arcy, 2000]). When recorded with large sensor arrays, it is also possible to derive spatial estimates of intracranial source activation (Michel et al., 2004). While there has been much progress in spatial source localization in recent years, relatively little is known about the potential clinical applications, particularly for higher perceptual and cognitive functions. One major barrier is the lack of a method for comparing individual spatial patterns to the norm. Here, we present a new method for characterizing individual source activation maps called the profile algorithm.

As a first test of the profile algorithm, we verified its performance on a prominent clinical EP application. Visual-evoked potentials (VEPs) are used in the evaluation of various neurological and visual pathologies ([Chiappa, 1997] and [Walsh et al., 2005]). The utility of VEPs is derived primarily from the temporal information available from the waveforms. Distributed source modeling of VEPs, however, allows for the visualization of the related intracranial activity in the visual cortex. In terms of validation, VEPs and the visual cortex provide a good framework to evaluate whether the spatial information can be used to detect and evaluate differences in individual brain function. A simple test of the profile algorithm in this case involves differences in myopic individuals with and without corrected vision.

1.2. Background

VEPs are signal-averaged waveforms that are derived from scalp-recorded EEG ([Chiappa, 1997] and [Walsh et al., 2005]). They are generated in response to any repetitive visual stimulus, typically a pattern-reversal checkerboard. VEPs are most commonly recorded from a small electrode array spanning the occipital region. They contain distinct components, such as the N75 and P100 (Odom et al., 2004).[1] When used in the clinic, they can provide a reliable and objective assessment of the integrity of the anterior visual pathways (optic nerves, optic chiasm, and optic tracts). Abnormalities in these pathways are typically manifested as a delay in the latency of the P100 component. The individual waveforms are considered to be "abnormal" if the latency of the P100 falls outside of a normative range (e.g., Sisto et al., 2005). Less emphasis is placed on the amplitude of the P100, but when it is measured, it is defined as the N75–P100 peak difference (Odom et al., 2004).

When EEG is recorded from high-density electrode arrays, it is possible to estimate the intracranial generators. This approach involves estimating the current sources through the use of inverse modeling methods that use either equivalent current dipoles or distributed source models ([Picton et al., 1995] and [Michel et al., 2004]). Assumptions are generally made (e.g., mathematical or anatomical constraints) in order to reduce the solution space, as an infinite number of sources could generate a given scalp topography. Using these methods, it has been

possible to investigate VEP generators.[2] The N75 has been localized to the primary and secondary visual cortices (Di Russo et al., 2005). While the location of the P100 generator(s) is more contentious, it is generally thought to arise from not only the primary and secondary visual cortices, also extends to visual association areas (Di Russo et al., 2005). Overall, the source estimation results show relatively good correspondence with estimates obtained through functional magnetic resonance imaging ([Bonmassar et al., 2001], [Martínez et al., 2001], [Moradi et al., 2003], [Vanni et al., 2004] and [Whittingstall et al., 2007]).

Source estimation techniques are also promising in terms of clinical assessment. From a practical standpoint, they are attractive due to ease of implementation, accessibility, and cost-effectiveness. In addition, with the advent of higher density sampling, more accurate localization algorithms, and realistic head models, there has been a recent surge in the number of clinical applications. In particular, the ability of distributed source models to provide activation maps is useful for characterizing changes secondary to neurological diseases (e.g., [Michel et al., 2004] and [Thatcher et al., 2005]). This application is especially appealing if it can be applied to disease related activation changes in higher perceptual and cognitive processing, which have relatively fewer assessment techniques compared to sensory and motor deficits.

One major challenge in the clinical implementation of distributed source localization relates to characterizing activation maps at the individual level. Many of the studies that employ source localization use grand average data. While analysis can be done using individual subject data, the variance between individuals is a problem. For instance, when differences in activation patterns occur between individuals, it is difficult to disentangle whether these differences are within the normal range or provide potentially valuable diagnostic information. This represents perhaps one of the greatest challenges to translating functional brain imaging advances into new clinical methods.

The problem can be defined in a practical way. The use of distributed source localization as a clinical tool requires that it be performed with individual patients in mind. Currently, however, there is no established method to determine whether an individual's spatial activation pattern is "normal." While work has been undertaken to create a normative database for EEG (Thatcher et al., 2005), similar methods for EPs (and ERPs) remain to be developed. One possible approach is to take advantage of the functional specificity of EPs by establishing a normative spatial profile of activation for a given function (i.e., identify a common activation pattern that occurs across individuals). Once established, a patient's spatial pattern can then be compared against this profile in order to assess whether it is consistent with the norm.

Our group has recently developed an algorithm that is effective at characterizing similarities across individual subjects' source localization maps (Marchand et al., 2008). In the current study, we test if this algorithm is capable of differentiating "normal" versus "abnormal" VEP activation patterns. The rationale is as follows: VEP components are representative of underlying visual activation and are similar in terms of latency and amplitude across individuals with intact visual processing (Odom et al., 2004). It is therefore reasonable to expect that, for a given VEP component, the corresponding source maps will show similarities across individuals. As such, for a group of subjects, it should be possible to estimate the pattern of source activity that is common to those subjects' VEP peaks. We refer to this common pattern of activation across

subjects as a profile for the given VEP component. Within a new test subject's series of source maps (derived from all time points in the waveform), the map that most closely matches the profile should correspond to that same VEP component. In other words, source maps that closely match the profile should be representative of the function(s) depicted in the profile. In contrast, source maps that do not match the profile should be representative of either different functions (i.e., a different component), or abnormal versions of the function(s) depicted in the profile.

1.3. Objectives and hypotheses

While there has been significant progress in the realm of functional imaging, there are limited methods for distinguishing "normal" from "abnormal" activation patterns at the individual level. The objective of this study was to validate a new method for comparing individual source activation maps against the norm. In order to establish the clinical utility, the method was first tested in terms of its performance on a well-established VEP diagnostic test.

We examined differences in visual activation by testing myopic individuals with corrected and uncorrected vision using a pattern-reversal checkerboard. In order to ensure that acuity affected how the stimuli were perceived, different check sizes were used. The first hypothesis predicted that the VEPs would vary as a function of visual condition and check size. The second hypothesis predicted that the profile algorithm would successfully differentiate source maps for corrected and uncorrected vision. Exploratory correlation analyses were also done to examine the relationship between the magnitude of visual impairment and the measurements of N75 and P100 amplitude as well as algorithm performance.

2. Materials and methods

2.1. Subjects

Twenty-five subjects participated in the study, with the data from two subjects excluded (one did not meet the inclusion criteria and the data from the other were corrupted by noise). The remaining 23 subjects (11 male and 12 female) had a mean age of 21.4 (SD = 3.9 years). Only subjects between 18 and 50 years of age were recruited, as the latency and amplitude of the P100 are known to change as a function of age (Tobimatsu, 1995). All subjects' binocular visual acuity was assessed using a Snellen visual acuity chart, and all had corrected-to-normal vision (20/20 or better) that was 20/40 or worse when uncorrected (mild visual impairment, as defined by Dandona and Dandona, 2006). Subjects indicated through self-report that their visual impairments were non-neurologic in nature. They also completed a general health screening questionnaire to screen for medical and psychiatric conditions that might affect performance on the task. The study had ethics approval, and all subjects provided informed consent prior to their participation.

2.2. Pattern-reversal VEP procedure

Stimuli consisted of alternating black and white checkerboards, with white check luminance > 80 cd m^{-2}, and the Michelson contrast at 99% ([Brigell et al., 1998] and [Odom et al., 2004]). Checkerboards subtended a visual angle of 17.67° (corresponding to the dimensions

of the screen used to present stimuli) and check size varied across three levels: small, medium, and large (5, 8.3, and 10 min of arc, respectively). The smallest check size corresponded to the size of the smallest discernable optotype when visual acuity is 20/20. The largest check size corresponded to the smallest check that can be seen when visual acuity is 20/40 (Colenbrander, 2001). The remaining check size was an intermediate between the largest and smallest checks such that the dimensions in pixels were whole numbers (i.e., the boundaries of the checks were not split across pixels). For each checkerboard, there were equal numbers of black and white checks, and a central fixation point consisting of a red dot.

Subjects viewed two runs of the checkerboard paradigm—one with corrected vision and one with uncorrected vision (counterbalanced order). Within each run, there were 15 blocks of checkerboard reversals, with 5 blocks of each check size presented in random order. Each block lasted 15 s with checkerboards reversing at 2 Hz, and was followed by a 5-s fixation, during which subjects indicated the size of the checks in the preceding block via a three button forced choice (to ensure continuous attention). All responses were made with the right hand.

2.3. Electrophysiological recordings and source localization

EEG data were recorded and analyzed using a 64-channel BrainAmpMR EEG system and BrainVision Recorder and Analyzer (Brain Products, GmbH). Electrodes (Ag/AgCl) were embedded in an Electro-Cap (Electro-Cap International, Inc) with their locations conforming to an extension of the International 10/20 System (American Electroencephalographic Society, 1991). All sites were referenced to an electrode on the nose. Vertical and horizontal electrooculograms were recorded from above and below the left eye, and at the outer canthi of both eyes, respectively. Impedances were maintained at or below 10 kΩ. Continuous EEG data were recorded with a sampling rate of 5 kHz, gain of 1000, and an online band-pass filter of 0.01–250 Hz.

The data were down-sampled offline to 1 kHz, and filtered to 0.1–30 Hz, with a 60-Hz notch filter.[3] To derive the VEPs, data were segmented using triggers that were time-locked to each checkerboard reversal (−100 to 500 ms) and baseline corrected (−100 to 0 ms). The data were re-referenced to Fz (Odom et al., 2004). There were 150 trials per condition. Trials with ocular artifacts were rejected with a threshold of ±75 μV, and remaining trials were averaged according to experimental condition. The average number of trials for corrected vision was 141.09 (SD = 11.09) for large checks, 139.74 (SD = 11.60) for medium checks, and 142.00 (SD = 9.59) for small checks. The average number of trials for uncorrected vision was 140.30 (SD = 10.70) for large checks, 140.13 (SD = 10.22) for medium checks, and 142.22 (SD = 8.68) for small checks. The N75 and P100 were automatically peak scored at Oz and manually verified (for each subject and each condition). The N75 was defined as the local minimum from 55 to 135 ms post-stimulus, and the P100 was defined as the local maximum from 90 to 170 ms post-stimulus. The P100 amplitude was calculated by taking the difference between the N75 and P100 amplitudes.

Distributed source modeling was performed using exact low-resolution electromagnetic tomography (eLORETA; Pascual-Marqui, 2007).[4] The eLORETA program uses the MNI152 template with a total of six-thousand two-hundred thirty-nine 5 mm^3 voxels. Source maps were created for each subject in all six conditions (2 levels of vision, 3 levels of check size). A

separate map was created for each time point in every VEP (0–500 ms) (i.e., 500 temporally ordered maps times 6 conditions times and 23 subjects, for a total of 69,000 maps).

2.4. Profile development

As previously described, a "profile" is a tomographical map that depicts inter-individual similarities across source maps corresponding to a specific component peak. For a given VEP component, a profile was created from the source maps that corresponded to each individual subject's component peak. To create the profile, different threshold filters were first applied to each of the peak source maps. This filter removed all but the most active voxels from each of the maps (i.e., 5, 10, 15, 20, or 25% most active voxels were kept). The voxels that remained in each map were then candidates for incorporation into the profile, and no longer contained information about activation intensity. In other terms, this binarization operation converted each voxel of the map as being either active (and relevant) or inactive (and therefore not used for the rest of the procedure). Only the active voxels that were candidates in more than 50% of the individual source maps were included in the profile (i.e., present in the absolute majority of all the participants).

For the purposes of this investigation, a 'leave-one-out' procedure was used, as is common in machine learning ([Stone, 1977] and [Weiss and Kulikowski, 1991]). For a given condition, a profile was created from all subjects except one. The remaining subject then served as the test subject. The procedure was repeated until each subject had served as the test subject, and profiles had been created from all sets of 22 subjects' peak source maps (i.e., $N − 1$).

Once a profile was constructed, it was compared to the test subject's temporally ordered series of source maps (the 500 maps that corresponded to every time point in their VEP). Each of the test subject's 500 maps underwent the same threshold filtering to remove all but the most active voxels from each map prior to comparison with the profile. For each map, a similarity index was calculated that measured the degree to which the map matched the profile (i.e., a binary matching decision). For each active voxel in the source map that matched the corresponding active voxel in the profile, the similarity index was incremented by one. The greater the degree of similarity between a map and the profile, the higher the similarity index. Once the similarity index had been calculated for each of the 500 maps, they were rank ordered. The map that had the highest similarity index was given a rank of 1, and all others followed in order of descending similarity. We report the rank of the source map corresponding to the component peak (relative to the other 499 maps).

The following pseudo-code describes the profile construction/rank ordering procedure.

```
For each component
    For each subject, (i = 1 to N)
        Build profile with remainder of subjects
        Similarity index = 0
        For each source map, of subject, (j = 1 to T)
            Calculate similarity index (map, profile),
            that is, increase the similarity index by 1
            for each voxel that is both active in the
            profile and the current map
        [End for]
        Sort maps, by descending similarity index
        Note rank order of peak map
    [End for]
[End for]
```

where N is the total number of subjects (in this study, 23) and T is the number of source maps per condition per subject (in this study, 500).

Thus, the success of the characterization was measured in terms of the rank of the map that corresponded to the test subject's component peak—the higher the rank of that particular map, the better the characterization. Due to the aforementioned leave-one-out procedure, 23 rank orders (one for each subject) were calculated for a given threshold filter. It was therefore possible to select the optimized threshold by using the one that was giving overall the minimal mean of these rank orders. Following this procedure, the optimal thresholds for the N75 and P100 were 20% and 25%, respectively.

In the current study, the algorithm was evaluated in terms of its ability to successfully characterize individual differences between "normal" and "abnormal" brain activation patterns. To do this, we used profiles derived from the corrected vision condition to rank order source maps from both the corrected and uncorrected vision conditions for each test subject. Profiles from the uncorrected vision condition were also evaluated in order to confirm that only correct maps could successfully differentiate the conditions. The entire procedure was implemented on both the N75 and the P100 for all three check sizes.

2.5. Statistical analyses

Repeated measures analyses of variance (ANOVAs) with factors of vision condition (corrected and uncorrected) and check size (small, medium, and large) were used in all analyses. These analyses included behavioural accuracy, N75 and P100 amplitudes and latencies, and profile algorithm rank order data. Post hoc tests were done where applicable using paired samples t-tests. Additional Pearson's correlations were done to compare the magnitude of the visual impairment (difference between corrected and uncorrected visual acuity) to both changes in the VEP component amplitudes and component rank orders. All analyses used corrected degrees of freedom (Greenhouse and Geisser, 1959) and required an alpha level of 0.05 for statistical significance.

2.6. Comparison between spatial profiling algorithm and ERP peak amplitude

Based on source localization maps, the profile method is by nature aimed at highlighting spatial information that likely allows a subject's condition to be differentiated, namely corrected versus uncorrected vision. While the spatial patterns can certainly complement ERPs measurements that are traditionally used, it is also worthwhile from both a validation and a practical perspective to investigate the respective discriminatory power of these two approaches. In other words, does the brain profiling method have greater discriminability than simply looking at ERP features?

To reply to this question, we first collected the peak amplitudes at Oz site of both the N75 and P100 components in the two conditions for all the 23 participants. Then, for each subject, we calculated the *z*-score of the rank order (for the profile method) and the amplitude (for the ERP method) using the corresponding normative distribution (i.e., the set of values gathered from the corrected vision condition). *z*-Scores allowed the two methods to be compared directly.

3. Results

3.1. Behavioural results

A repeated measures ANOVA revealed a main effect of vision condition on response accuracy ($F(1,22) = 5.714$, $p < 0.05$) with higher accuracy for corrected vision (mean = 0.92, SD = 0.01) than uncorrected vision (mean = 0.86, SD = 0.03). There was also a main effect of check size on accuracy ($F(2,22) = 4.774$, $p < 0.05$). Post hoc *t*-tests showed that there was a significant difference in accuracy for small and medium checks ($t(45) = -3.382$, $p < 0.001$), with higher accuracy for small checks (mean = 0.93, SD = 0.12) than medium checks (mean = 0.86, SD = 0.18).

3.2. Electrophysiological results

Fig. 1 depicts the grand average waveforms at Oz for corrected (A) and uncorrected (B) vision. Repeated measures ANOVAs were used to analyze effects of vision condition and check size on the latency and amplitude of the VEP components. These results are described below and summarized in [Table 1A] and [Table 1B], respectively.
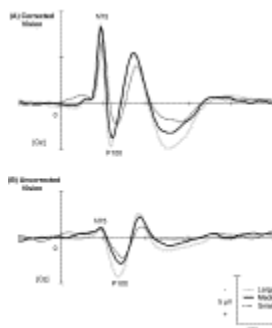
Full-size image (30K)

Fig. 1.

Grand averaged ($N = 23$) pattern-reversal VEPs showing effect of visual condition (corrected and uncorrected) and check size (small, medium, large) at Oz. The N75 and P100 are indicated on the waveforms. Time (ms) is on the horizontal axes (hatch marks every 100 ms) and amplitude (μV) is on the vertical axes (hatch marks every 5 μV). Note that negative is plotted up.

Table 1A. Latency ANOVA results.

	df	F	p
N75			
Vision	1, 22	19.478	<0.001
Check size	2, 22	2.686	>0.05
Vision × check size	2, 22	0.295	>0.05
P100			
Vision	1, 22	14.886	<0.001
Check size	2, 22	17.311	<0.001
Vision × check size	2, 22	0.663	>0.05

Table 1B. Amplitude ANOVA results.

	df	F	p

	df	F	p
N75			
Vision	1, 22	27.328	<0.001
Check size	2, 22	2.328	>0.05
Vision × check size	2, 22	3.834	<0.05
P100			
Vision	1, 22	18.015	<0.001
Check size	2, 22	10.581	<0.001
Vision × check size	2, 22	4.248	<0.05

The N75 was significantly earlier and had significantly greater amplitude for corrected vision than uncorrected vision ($p < 0.001$). There was also a vision condition × check size effect on N75 amplitude ($p < 0.05$). Post hoc t-tests showed that the amplitude was consistent across all check sizes for uncorrected vision, but was larger for both large and medium checks relative to small checks for corrected vision ($p < 0.05$).

The P100 was also earlier and had greater amplitude for corrected vision ($p < 0.001$). There was a main effect of check size on latency ($p < 0.001$), where the P100 was significantly later for small checks than both medium and large checks ($p < 0.05$). It was also later for medium checks than for large checks ($p < 0.05$). There was a main effect of check size on P100 amplitude ($p < 0.001$), and post hoc t-tests showed that the amplitude was significantly greater for large checks than either small or medium checks ($p < 0.01$). Finally, there was a vision condition × check size interaction on amplitude ($p < 0.05$), with increasing amplitude as a function of check size for corrected vision only. Scalp topology maps for the N75 and P100 in the corrected and uncorrected vision conditions are presented in Fig. 2.
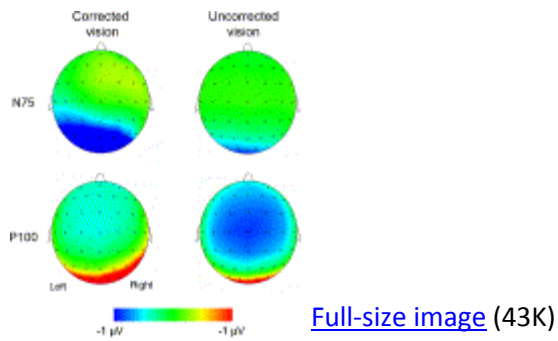
Fig. 2.

Grand averaged ($N = 23$) scalp topology maps for the N75 and P100 in the corrected and uncorrected vision conditions.

3.3. Source localization results

Grand average source localization maps from the corrected and uncorrected conditions are shown for the N75 and P100 in [Fig. 3] and [Fig. 4], respectively (collapsed across check size). In the corrected vision condition, the N75 was localized to the primary and secondary visual cortices, whereas the P100 was localized to secondary and association visual cortices. Note that the source maps for the N75 are displayed using separate scale bars for corrected $(5.0 \times 10^{-2} \ \mu A/mm^2)$ and uncorrected vision $(3.0 \times 10^{-3} \ \mu A/mm^2)$. If both were shown on the same scale, there would be no visible activation in the uncorrected vision condition. In contrast to the N75, the source maps for the P100 are displayed using the same scale for both vision conditions $(1.5 \times 10^{-2} \ \mu A/mm^2)$.
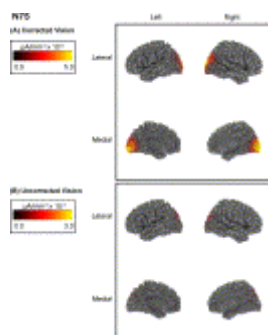

Fig. 3.

Grand averaged ($N = 23$) eLORETA source maps of the N75 in the corrected and uncorrected vision conditions (lateral and medial views). The scale bar represents the activation intensity ($\mu A/mm^{-2}$). Note there are two different scale bars—one for corrected vision and one for uncorrected vision.
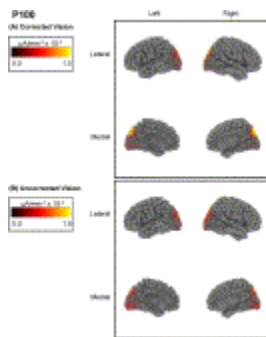

Fig. 4.

Grand averaged ($N = 23$) eLORETA activation maps of the P100 in the corrected and uncorrected vision conditions. All other details as in Fig. 3.

3.4. Profile results

A repeated measures ANOVA was used to analyze the profile algorithm's ability to differentiate between corrected and uncorrected conditions for all three check sizes. Profiles were constructed from N75 and P100 source maps in the corrected vision condition.[5] Fig. 5 presents profiles for the N75 and P100 (constructed from all 23 subjects).
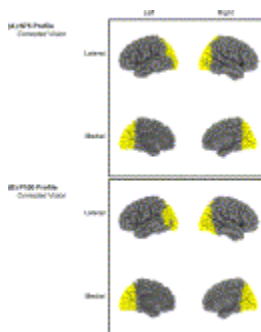

Fig. 5.

Sample corrected vision profiles for the N75 (A) and P100 (B) constructed from all 23 subjects. Voxels included in the profile are indicated in yellow.

For the N75, the profile algorithm ranked the corrected vision map higher than the uncorrected vision map for 20 out of 23 subjects (87%). This result was supported by the ANOVA, which revealed a main effect of vision ($F(1,22) = 30.217$, $p < 0.001$). Specifically, corrected N75 maps were ranked significantly higher (mean rank order = 52.8, SD = 15.6) than uncorrected N75 maps (mean rank order = 186.7, SD = 20.8). There was no other significant effect. The N75 rank order plot, collapsed across check sizes, is shown in Fig. 6.
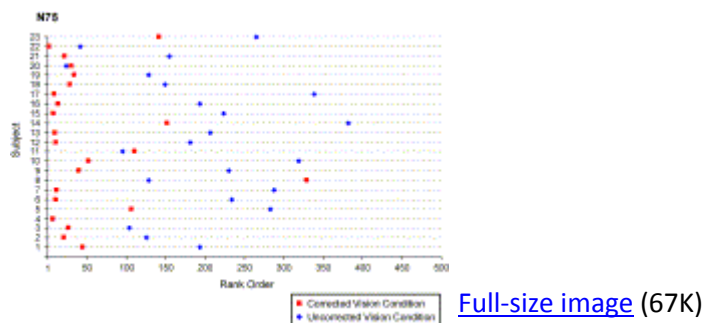

Full-size image (67K)

Fig. 6.

Rank order plots of N75 source maps collapsed across check sizes. A corrected profile was used to rank order corrected (red square) and uncorrected (blue diamond) source maps for all subjects ($N = 23$). Rank order is plotted on the horizontal axes and subjects 1–23 are plotted on the vertical axes.

For the P100, the profile algorithm ranked the corrected vision map higher than the uncorrected vision map for 7 out of 23 subjects (30%). There was no significant difference in the profile algorithm's ability to differentiate between corrected and uncorrected conditions. Corrected vision P100 maps were ranked as 83.9 (SD = 106.9) and uncorrected vision P100 maps were ranked as 96.9 (SD = 85.0). The P100 rank order plot, collapsed across check sizes, is shown in Fig. 7.
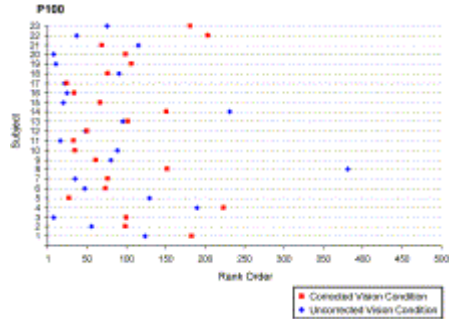
Fig. 7.

Rank order plots of P100 source maps collapsed across check sizes. All other details as in Fig. 6.

3.5. Correlation results

Correlation analyses were done to compare the magnitude of visual impairment to changes in VEP component amplitudes (corrected–uncorrected) and component rank orders (for all check sizes). For VEP component amplitudes (corrected–uncorrected), only the P100 was significantly, positively correlated with magnitude of visual impairment ($r = 0.48$, $p < 0.05$, large checks, see Fig. 8), such that larger P100 changes between the corrected and uncorrected vision conditions were observed for individuals with greater visual impairment.
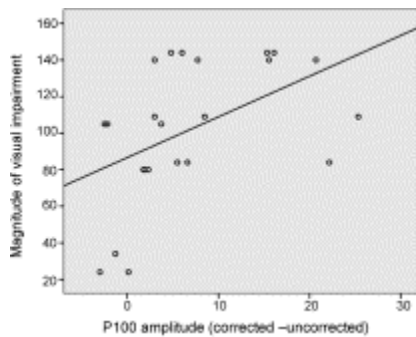

Fig. 8.

Scatter plot of visual impairment magnitude and the P100 amplitude (corrected–uncorrected) for large checks.

For rank order (corrected–uncorrected), the P100 was significantly, negatively correlated with magnitude of visual impairment ($r = -0.57$, $p < 0.01$, medium checks, see Fig. 9), such that smaller rank order differences between the corrected and uncorrected vision conditions were observed for individuals with greater visual impairment. There was no other significant correlation.
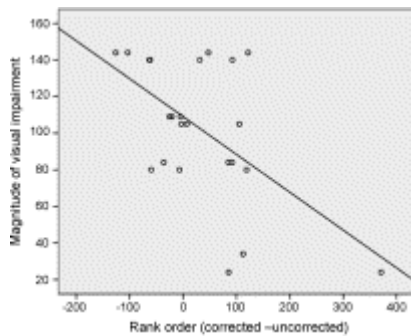

Fig. 9.

Scatter plot of visual impairment magnitude and the P100 rank order (corrected–uncorrected) for medium checks.

3.6. Comparison between spatial profiling algorithm and ERP peak amplitude

In order to evaluate whether the spatial profiling algorithm provides improved discriminability between conditions, we also evaluated the performance of a method using the peak amplitude to distinguish between the conditions. The results of this analysis are shown in Table 2. For both the spatial profiling algorithm and the peak amplitude method, the N75 results better differentiate the two conditions. Furthermore, regardless the ERP component of interest, the profile procedure outperforms the corresponding ERP peak amplitude method. This advantage is statistically significant for the N75. Thus, not only does the profile method have the potential to give valuable insight regarding the spatial patterns of activation, but it also improves discriminatory power.

Table 2. For each subject, the difference (as a z-score) between their corrected and uncorrected vision conditions for the N75 and P100 results for both the peak amplitude method and the profiling algorithm (rank order) method.

Subject	N75	P100

	Amplitude	Rank order	Amplitude	Rank order
1	1.33	1.92	0.18	0.47
2	0.91	1.0	−0.09	−0.71
3	1.01	0.69	0.13	−1.54
4	−0.32	−0.64	−0.77	1.61
5	1.32	3.15	−0.22	0.56
6	1.17	2.49	−0.27	−0.86
7	1.27	3.22	0.13	−1.08
8	1.34	1.04	0.34	4.93
9	1.06	2.44	−0.42	−0.29
10	1.21	3.65	0.19	−0.15
11	1.16	0.59	0.26	−1.4
12	1.00	1.76	0.41	−0.85
13	0.93	2.11	−0.51	−0.02
14	1.17	4.51	−0.6	2.32
15	1.15	2.34	−1.01	−1.33
16	1.17	1.93	0.2	−1.25

Subject	N75		P100	
	Amplitude	Rank order	Amplitude	Rank order
17	1.31	3.92	0.62	−1.3
18	1.21	1.32	−0.11	−0.11
19	1.13	1.03	0.44	−1.5
20	0.30	−0.4	0.97	−1.54
21	1.22	1.4	−0.43	0.31
22	−0.24	−0.16	0.36	−1.03
23	1.34	2.9	0.34	−0.38
Mean (SD)	1.01 (0.46)	1.83 (1.37)	0.01 (0.48)	−0.22 (1.51)
Wilcoxon test	$T = 44$, $p < 0.05$		$T = 89$, $p = 0.22$	

4. Discussion

4.1. Summary of results

In the current study, we investigated a new method called the profile algorithm. The algorithm compared individual spatial EP/ERP activation to the norm. The primary objective was to validate the method using well-established VEPs. We tested for individual differences in the spatial activation of myopic individuals with corrected versus uncorrected vision. As expected, latency and amplitude for the N75 and P100 varied significantly as a function of visual acuity and check size (hypothesis 1). The profile algorithm also successfully differentiated source maps for corrected and uncorrected conditions (hypothesis 2). However, this occurred only for the N75 and not for the P100. Ostensibly, examination of the P100 rank scores suggested that the method performed equally well for corrected and uncorrected vision. However, exploratory correlation

analyses suggested that changes in the P100 may in fact be sensitive to differences in visual acuity. Specifically, the P100 rank order was negatively correlated with magnitude of visual deficit (i.e., larger rank order differences with smaller visual deficits). While preliminary, the pattern of N75 and P100 results suggests that unique and non-redundant information can be obtained from the spatial data.

4.2. ERP findings

The VEP waveform results are consistent with changes that occur as a result of deficits in visual acuity. Specifically, N75 and P100 latencies were delayed and amplitudes were reduced in the uncorrected vision condition (Fig. 1). Moreover, the P100 amplitude changes correlated positively with the magnitude of visual deficit. The results are in general agreement with studies of patients who have problems with visual acuity secondary to conditions such as diabetes and glaucoma (e.g., [Alessandrini et al., 2001] and [Parisi, 2001]). While changes in component amplitudes tend to be less well characterized, decreases in VEP amplitudes have also been reported in diabetes and multiple sclerosis (e.g., [Alessandrini et al., 2001] and [Leys et al., 1991]).

4.3. Source estimation findings

The source estimation results showed that both the N75 and P100 localized to the visual cortex ([Fig. 2] and [Fig. 3]). Interestingly, the regions identified using source analysis were consistent with the profiles calculated for the N75 and P100 (Fig. 4), although the extent of activation was smaller in the source analysis results. The larger extent of activation in the profile likely results from the variability in the activation patterns across subjects.

4.4. The profiling algorithm and potential clinical applications

The normative comparison represents a critical feature of the method. Of note, the N75 was able to distinguish between the spatial patterns of the corrected versus uncorrected visual acuity conditions, whereas, the differences were not significant for the P100. This pattern is consistent with the relative performance of the N75 and P100 when component amplitudes are examined (Table 2). It is possible that the P100 is relatively insensitive to changes to the visual input associated with the acuity manipulation. The issue of choosing an appropriate component for a given application is discussed further in Section 4.5.

Importantly, we found that the spatial profiling algorithm was better able to distinguish between normal and abnormal than ERP amplitude methods (see Table 2). This provides strong evidence for the benefits of using our spatial profiling method over using ERPs to distinguish between normal versus abnormal brain processing. However, more work is needed to evaluate our method's performance relative to other classification techniques (e.g., topographic ERP analyses using independent component analysis or *k*-mean clustering; Murray et al., 2008). It is worth noting that our method has an inherent advantage of being relatively computationally inexpensive.

Spatial EP/ERP information represents a potentially valuable tool for developing clinical diagnostics, particularly for higher perceptual and cognitive functions. Historically, ERPs have been limited in terms of their use in clinical realms (e.g., [Connolly et al., 2000] and [D'Arcy et al., 2003]). This has, in part, been due to the need to identify appropriate applications for ERP components. Nonetheless, the functional significance and anatomical correlates of components like the semantic N400 are becoming increasingly well characterized ([D'Arcy et al., 2004] and [D'Arcy et al., 2005]). Changes in the spatial activation pattern of a component like the N400 represent a relatively untapped area for clinical development (e.g., biomarker identification). The underlying premise is to first better isolate the process using the temporal resolution of ERPs and then detect whether there are changes in the underlying functional neuroanatomy for that cognitive process (at the individual level). As such, the profile algorithm has the potential to add unique and valuable information to the evaluation of perceptual and cognitive processes in a clinical setting.

4.5. Future work

In order to apply this method to distinguish between normal versus abnormal brain processing for a given function, it is crucial to both design an appropriate experiment and investigate the appropriate ERP component. The relative utility of the N75 and the P100 for distinguishing between corrected versus uncorrected vision in the current work highlights the importance of the component being studied to the success of the approach.

In the current study, we focused on using the profile algorithm to predict which map corresponded to the peak of the ERP component. However, it is also possible to use the profile algorithm to evaluate how similar the maps corresponding to other time points are to the profile. This approach might provide information on the sequence of processing phases during a given function. In addition, future work investigating whether the profile algorithm can be meaningfully applied to the generators of frequency components could further expand the breadth of potential applications (see Thatcher et al., 2005, for related work using LORETA to localize frequency generators for the purpose of creating a normative database).

5. Significance

The findings provide strong support for the profile algorithm's ability to normatively evaluate VEP spatial activation maps. Importantly, this method creates the potential for new avenues of research on spatial changes in the network that supports perceptual and higher cognitive functions. A number of ERP components exist in which the spatial activation may prove valuable for the assessment and monitoring of brain diseases and disorders (e.g., the N400 in stroke). While the temporal domain has been much studied for clinical benefit, the spatial domain in EPs/ERPs (and magnetoencephalography) remains largely unexplored. Methods such as the spatial profiling algorithm may indeed provide the means to further investigation.

Acknowledgements

References

Alessandrini et al., 2001 M. Alessandrini, E. Bruno, V. Parisi, L. Uccioli and P.G. Giacomini, Saccadic eye movement and visual pathways function in diabetic patients, *An Otorrinolaringol Ibero Am* **28** (2001), pp. 269–280.

AES, 1991 American Electroencephalographic Society, Guidelines for standard electrode position nomenclature, *J Clin Neurophysiol* **8** (1991), pp. 200–202.

Bonmassar et al., 2001 G. Bonmassar, D.P. Schwartz, A.K. Liu, K.K. Kwong, A.M. Dale and J.W. Belliveau, Spatiotemporal brain imaging of visual-evoked activity using interleaved EEG and fMRI recordings, *NeuroImage* **13** (2001), pp. 1035–1043.

Brigell et al., 1998 M. Brigell, M. Bach, C. Barber, K. Kawasaki and A. Kooijman, Guidelines for calibration of stimulus and recording parameters used in clinical electrophysiology of vision, *Doc Ophthalmol* **95** (1998), pp. 1–14.

Chiappa, 1997 K.H. Chiappa, Evoked potentials in clinical medicine (3rd ed.), Lippincott–Raven, Philadelphia (1997).

Colenbrander, 2001 A. Colenbrander, Measuring vision and vision loss. In: W. Tasman and E.A. Jaeger, Editors, *Duane's clinical ophthalmology* **vol. 5**, Lippincott Williams & Wilkins, Philadelphia (2001).

Connolly and D'Arcy, 2000 J. Connolly and R.C.N. D'Arcy, Innovations in neuropsychological assessment using event-related brain potentials, *Int J Psychophysiol* **37** (2000), pp. 31–47.

Connolly et al., 2000 J.F. Connolly, R.C.N. D'Arcy, R.L. Newman and R. Kemps, The application of cognitive event-related brain potentials in language-impaired individuals: Review and case studies, *Int J Psychophysiol* **38** (2000), pp. 55–70.

D'Arcy et al., 2003 R.C.N. D'Arcy, Y. Marchand, G.A. Eskes, E.R. Harrison, A. Major, S.J. Phillips and J.F. Connolly, Electrophysiological assessment of language function following stroke, *Clin Neurophys* **114** (2003), pp. 662–672.

Dandona and Dandona, 2006 L. Dandona and R. Dandona, Revision of visual impairment definitions in the international statistical classification of diseases, *BMC Med* **4** (2006), p. 6.

D'Arcy et al., 2004 R.C.N. D'Arcy, J.F. Connolly, E. Service, C.S. Hawco and M.E. Houlihan, Separating phonological and semantic processing in auditory sentence processing: a high-resolution event-related brain potential study, *Hum Brain Mapp* **22** (2004), pp. 40–51.

D'Arcy et al., 2005 R.C.N. D'Arcy, E. Service, J.F. Connolly and C.S. Hawco, The influences of increased working memory load on semantic neural systems: a high-resolution event-related brain potential study, *Brain Res* **22** (2005), pp. 177–191.

Di Russo et al., 2005 F. Di Russo, S. Pitzalis, G. Spitoni, T. Aprile, F. Patria and D. Spinelli *et al.*, Identification of the neural sources of the pattern-reversal VEP, *NeuroImage* **24** (2005), pp. 874–886.

Greenhouse and Geisser, 1959 S.W. Greenhouse and S. Geisser, On methods in the analysis of profile data, *Psychometrika* **24** (1959), pp. 95–112.

Hashimoto et al., 1999 T. Hashimoto, S. Kashii, M. Kikuchi, Y. Honda, T. Nagamine and H. Shibasaki, Temporal profile of visual evoked responses to pattern-reversal stimulation analyzed with a whole-head magnetometer, *Exp Brain Res* **125** (1999), pp. 375–382.

Leys et al., 1991 M.J.J. Leys, C.M.L.J. Candaele, A.F. De Rouck and J.V. Odom, Detection of hidden visual loss in multiple sclerosis, *Doc Ophthalmol* **77** (1991), pp. 255–264.

Luck, 2005 S.J. Luck, An introduction to the event-related potential technique, MIT Press, Cambridge (2005).

Marchand et al., 2008 Y. Marchand, R.C.N. D'Arcy, V.L. Versteeg and E.L. Mazerolle, Profiling brain function for source imaging in EEG and MEG: a similarity ranking method for evaluating individual activation, *Proceedings of the 14th annual meeting of the organization for human brain mapping* (2008), p. S53.

Martínez et al., 2001 A. Martínez, F. DiRusso, L. Anllo-Vento, M.I. Sereno, R.B. Buxton and S.A. Hillyard, Putting spatial attention on the map: timing and localization of stimulus selection processes in striate and extrastriate visual areas, *Vision Res* **41** (2001), pp. 1437–1457.

Michel et al., 2004 C.M. Michel, M.M. Murray, G. Lantz, S. Gonzalez, L. Spinelli and R. Grave de Peralta, EEG source imaging, *Clin Neurophys* **115** (2004), pp. 2195–2222.

Moradi et al., 2003 F. Moradi, L. Liu, K. Cheng, R. Waggoner, K. Tanaka and A. Ioannides, Consistent and precise localization of brain activity in human primary visual cortex by MEG and fMRI, *NeuroImage* **18** (2003), pp. 595–609.

Murray et al., 2008 M.M. Murray, D. Brunet and C.M. Michel, Topographic ERP analysis: a step-by-step tutorial review, *Brain Topogr* **20** (2008), pp. 249–264.

Nakamura et al., 1997 A. Nakamura, R. Kakigi, M. Hoshiyama, K. Sachiko, Y. Kitamura and M. Shimojo, Visual evoked magnetic fields to pattern reversal stimulation, *Brain Res Cogn Brain Res* **6** (1997), pp. 9–22.

Odom et al., 2004 J.V. Odom, M. Bach, C. Barber, M. Brigell, M.F. Marmor and A. Patrizia Tormene *et al.*, Visual evoked potentials standard (2004), *Doc Ophthalmol* **108** (2004), pp. 115–123.

Parisi, 2001 V. Parisi, Impaired visual function in glaucoma, *Clin Neurophysiol* **112** (2001), pp. 351–358.

Pascual-Marqui, 2007 Pascual-Marqui, Pascual-Marqui RD. Discrete, 3D distributed, linear imaging method of neuronal activity. Part 1. Exact, zero error localization. arXiv:0710.3341 [math-ph], http://arxiv.org/pdf/0710.3341 [17.10.07].

Picton et al., 1995 T.W. Picton, O. Lins and M. Scherg, The recording and analysis of event-related potentials. In: R. Johnson, Editor, *Handbook of neuropsychology*, Elsevier, Amsterdam (1995), pp. 429–499.

Sisto et al., 2005 D. Sisto, M. Trojano, M. Vetrugno, T. Trabucco, G. Iliceto and C. Sborgia, Subclinical visual involvement in multiple sclerosis: a study by MRI, VEPs, frequency-doubling perimetry, standard perimetry, and contrast sensitivity, *Invest Ophthalmol Vis Sci* **46** (2005), pp. 1264–1268.

Stone, 1977 M. Stone, An asymptotic equivalence of choice of model by cross-validation and Akaike's Criterion, *J R Stat Soc* **38** (1977), pp. 44–47.

Thatcher et al., 2005 R.W. Thatcher, D. North and C. Biver, Evaluation and validity of a LORETA normative EEG database, *Clin EEG Neurosci* **36** (2005), pp. 116–122.

Tobimatsu, 1995 S. Tobimatsu, Aging and pattern visual evoked potentials, *Optom Vis Sci* **72** (1995), pp. 192–197. **Full Text** via CrossRef | View Record in Scopus | Cited By in Scopus (13)

Vanni et al., 2001 S. Vanni, T. Tanskanen, M. Seppä, K. Uutela and R. Hari, Coinciding early activation of the human primary visual cortex and anteromedial cuneus, *Proc Natl Acad Sci U S A* **98** (2001), pp. 2776–2780.

Vanni et al., 2004 S. Vanni, J. Warnking, M. Dojat, C. Delon-Martin, J. Bullier and C. Segebarth, Sequence of pattern onset responses in the human visual areas: an fMRI constrained VEP source analysis, *NeuroImage* **21** (2004), pp. 801–817.

Walsh et al., 2005 P. Walsh, N. Kane and S. Butler, The clinical role of evoked potentials, *J Neurol Neurosurg Psychiatry* **76** (2005), pp. 16–22.

Weiss and Kulikowski, 1991 S.M. Weiss and C.A. Kulikowski, Computer systems that learn, Morgan Kaufman, San Francisco (1991).

Whittingstall et al., 2007 K. Whittingstall, G. Stroink and M. Schmidt, Evaluating the spatial relationship of event-related potential and functional MRI sources in the primary visual cortex, *Hum Brain Mapp* **28** (2007), pp. 134–142.

[1] VEPs also contain later components, namely the N135 and the P200 ([Odom et al., 2004] and [Luck, 2005]). The current study restricted the focus to the N75 and P100, as these are the primary components used in clinical assessment.

[2] Similar work has been done using magnetoencephalography (MEG) with a consistent pattern of results (e.g., [Nakamura et al., 1997], [Hashimoto et al., 1999] and [Vanni et al., 2001]).

[3] A notch filter was used because the 24-dB roll-off on the low-pass filter extends past 60-Hz.

[4] A number of different source modeling approaches exist. Any distributed source modeling approach can be applied using the current method. We used eLORETA because it was the latest version of a frequently applied source modeling approach.

[5] Visual inspection of the results from profiles constructed from source maps in the uncorrected vision condition confirmed that neither the N75 nor the P100 could be characterized successfully.